

**N78-24063**

**ANALYTICAL MODELING OF UNDER-THE-WING EXTERNALLY BLOWN**

**FLAP POWERED-LIFT NOISE**

Daniel J. McKinzie, Jr.  
NASA Lewis Research Center

**SUMMARY**

The sound field produced by the interaction of a subsonic jet with a large-scale model of the under-the-wing externally blown flap in an approach attitude was analyzed. The analysis was performed to obtain a better understanding of the dominant noise sources and the mechanisms governing the peak sound-pressure-level frequencies of the broadband spectra. An analytical expression is derived which incorporates two available theories and experimental data; the expression predicts the sound field along a circular arc of approximately  $120^\circ$  measured from the upstream jet axis in the fly-over plane. The analysis compares favorably with test results obtained from two large-scale models, one using cold air from a conical nozzle and the other using hot gas from a TF-34 turbofan engine having a conical exhaust nozzle with a 12-lobe internal forced mixer. The frequency at which the peak sound pressure level occurs appears to be governed by a phenomenon which produces periodic formation and shedding of large-scale turbulence structures from the nozzle lip.

**INTRODUCTION**

The engine exhaust of the under-the-wing (UTW) externally blown flap (EBF) short takeoff and landing (STOL) aircraft is deflected downward by the wing flaps during takeoff and approach. Noise levels from 10 to 18 decibels greater than the jet noise are generated by the impingement of the jet on the flap surfaces (refs. 1 and 2).

NASA has conducted experimental research and development work to measure and define the flap interaction noise field for a variety of UTW configurations, as discussed in reference 3. After a review of the noise characteristics produced by each configuration, reference 3 notes that the overall sound pressure level was dependent on the sixth power of the peak impingement velocity and on the first power of the impingement area for each of these configurations. Thus, the dominant noise sources were not significantly altered or eliminated by the differences in the configurations. These results established a need for greater understanding of the dominant noise source mechanisms

in order to help develop noise suppression techniques that might be used to reduce the noise sources and thus meet noise goals.

In references 4 and 5 presentations are made of correlation and scaling-law techniques used to predict jet flap interaction noise for UTW EBF configurations. Although these techniques are presented as functions of geometric and gas dynamic variables, they do not adequately explain how or by what mechanisms the sound is produced. In reference 6 however, a mechanistic approach is taken in analyzing the noise generated by the interaction of a jet exhaust impinging on flat and curved plates. This approach is extended in reference 7 to large-scale test results of a UTW EBF configuration in which active and passive noise suppression techniques were studied.

The primary objective of this paper is to present, in summary form, the results of the UTW EBF analysis reported in reference 7 and to compare calculated estimates of the overall sound pressure level with two sets of test results. One set of data was obtained from a large-scale two-flap, non-swept-wing, cold-flow model of a UTW EBF configuration in an approach attitude (fig. 1). The second set of data was obtained from a full-scale, three-flap, swept-wing version of a UTW EBF configuration in an approach attitude using a TF-34 turbofan engine (ref. 8).

Although the prediction of the sound directivity for the UTW EBF takeoff configuration is not considered in this paper, the models of the noise sources presented are believed qualitatively applicable to the takeoff configuration.

#### SYMBOLS

$A$	actual correlation area, $m^2$
$A_c$	ideal correlation area, $m^2$
$(C_L)_{\nu}$	steady-state effective lift coefficient slope, $deg^{-1}$
$c$	speed of sound, m/sec
$D$	nozzle exit diameter, m
$F_L$	fluctuating lift force, N (fig. 4)
$f$	frequency, Hz
$f_T$	characteristic frequency of fluctuating lift forces, Hz
$M_j$	jet exit Mach number
$M_z$	local Mach number evaluated on jet axis

N	magnitude of velocity exponent
OASPL	overall sound pressure level, dB re $20 \mu\text{N}/\text{m}^2$
$P_{\text{ref}}$	reference sound pressure, $20 \mu\text{N}/\text{m}^2$
r	distance between observer and trailing edge, m (fig. 3)
SPL	sound pressure level, dB re $20 \mu\text{N}/\text{m}^2$
U	mean flow velocity, m/sec
$U_l$	local mean flow velocity evaluated on jet axis, m/sec
$U_m$	maximum mean velocity of free shear layer at trailing edge of flap, m/sec (fig. 3)
$v'/U_l$	turbulence intensity in direction normal to airfoil chord and leading edge
W	one-half of spanwise width of velocity profile between points where local velocity is equal to $U_m/2$ at trailing edge of flap, m (fig. 3)
x, y, z	Cartesian coordinates (fig. 3)
$\alpha$	normalized turbulence intensity (ref. 11)
$\beta$	angle between fluctuating force vector and observer, deg (fig. 4)
$\delta$	thickness of boundary layer, m (fig. 3)
$\theta$	radiation angle measured from nozzle inlet axis, deg (fig. 5)
$\rho$	density of undisturbed fluid, $\text{kg}/\text{m}^3$
$\rho_l$	density of fluid evaluated at point where $U_l$ is determined, $\text{kg}/\text{m}^3$
$\varphi$	angle, deg (fig. 3)
$\psi$	angle, deg (fig. 3)

Subscripts:

impact	impact
impinge	impingement
inflow	inflow
j	jet exit condition
l	local
TL	trailing edge

## ANALYSIS OF JET-FLAP-INTERACTION NOISE

In figure 2 the jet impingement on an EBF two-flap wing in an approach attitude is depicted by the dashed lines. The major noise sources, shown in figure 2, are assumed to be the result of oblique jet impingement, surface scrubbing, jet interaction with the leading and trailing edges, free shear layer mixing over the surface of the deflected flaps, and inflow about the most downstream (second) flap.

In reference 6, the noise resulting from oblique jet impingement, surface scrubbing, and free shear-layer mixing is termed impact noise. Impact noise  $OASPL_{\text{impact}}$  is defined as all the noise produced on a flat surface that is sufficiently large to exclude leading- and trailing-edge noise. The noise produced by inflow about the wing or flaps is referred to in this paper as inflow noise. Leading-edge noise is not considered because it is estimated to be less than trailing-edge noise, as reported in reference 9. Thus, it is assumed that trailing-edge noise, impact noise, and inflow noise are dominant. By assuming that these sound sources are uncorrelated (as proposed in refs. 6, 7, and 10), one may approximate their combined sound field by superposition. Therefore, the total jet-flap impingement OASPL is expressed as the logarithmic sum of the impact, trailing-edge, and inflow contributions:

$$OASPL_{\text{impinge}} = 10 \log \left[ 10 \exp \left( \frac{OASPL_{\text{impact}}}{10} \right) + 10 \exp \left( \frac{OASPL_{\text{TE}}}{10} \right) + 10 \exp \left( \frac{OASPL_{\text{inflow}}}{10} \right) \right] \quad (1)$$

This summation is referred to in this paper as impingement noise. The following sections present analytical expressions (in SI units) used to estimate trailing-edge, inflow, and impact noise.

### Trailing-Edge Noise

Trailing-edge noise may be estimated from the theoretical approach of reference 11 in the form presented in reference 6, where the details of the derivation are presented. This noise source has a velocity dependence of  $U^5$ . Figure 3 is a sketch, used in the derivation of reference 6, which shows the coordinate system. The overall sound pressure level of trailing-edge noise  $OASPL_{\text{TE}}$  for zero sweep angle is given (ref. 6) as follows:

$$\text{OASPL}_{\text{TE}} = 10 \log \frac{W \delta U_m^5}{r^2} + 10 \log \cos^2 \frac{\psi}{2} + 10 \log \frac{1.15 \times 10^8 \alpha^2 \rho^2}{c} \quad (2)$$

The angle  $\psi$  was determined graphically in reference 6 as a function of the acoustic radiation angle  $\theta$ .

### Inflow Noise

A derivation of the noise produced from inflow effects is given in reference 7. The derivation is based on reference 12, in which the large-scale turbulence structures of the jet flow field (ring vortices) are assumed responsible for what is referred to as inflow noise. Figure 4 is a sketch of the coordinate system used in the derivation of reference 7. The overall sound pressure of inflow noise  $\text{OASPL}_{\text{inflow}}$  is given in reference 7 as follows:

$$\begin{aligned} \text{OASPL}_{\text{inflow}} = & 10 \log \left[ \frac{(C_L) \rho_l U_l^2}{r} \right]^2 + 10 \log \left( A_c \frac{A}{A_c} \right) \\ & + 10 \log \left[ \frac{A}{A_c} \left( \frac{\pi}{7.559 + 1} \right) \right] + 10 \log \left[ \frac{\left( \frac{v}{U_l} \right)^2}{8\pi P_{\text{ref}}} \right]^2 \\ & + 10 \log \cos^2 \beta + 10 \log(0.23 f_p) \end{aligned} \quad (3)$$

The angle  $\beta$  was determined graphically in reference 7 as a function of the acoustic radiation angle  $\theta$ .

### Impact Noise

Although the specific mechanism which produces impact noise is not known, it is assumed as in reference 6 that impact noise is produced, in part, by the large-scale turbulence structures of the jet flow field impacting the flaps. In reference 13 the noise field produced when a 5.2-centimeter-diameter jet impacts a very large smooth flat board is presented. In the absence of an explicit theoretical expression and as

proposed in reference 6, these small-scale test results of reference 13, reproduced in figure 5, were used to estimate impact noise. The noise data shown in figure 5 did not include leading- and trailing-edge noise, but did include the remaining noise sources (i. e., oblique jet impingement coupled with surface viscosity effects, surface scrubbing, reflection by the surface, free jet mixing, and free shear-layer mixing over the deflected flat surface). The test conditions of reference 13 included nondimensional geometric and fluid flow conditions similar to those of the cold-flow test described in this paper. Therefore, the data of reference 13 were used after interpolation for the appropriate Mach number and normalized for differences in nozzle diameter  $D$  and microphone location  $r$  according to geometric scaling laws of reference 14.

#### COMPARISON OF CALCULATED AND MEASURED JET-FLAP-INTERACTION NOISE

Overall sound pressure levels representing the total jet-flap impingement noise (eq. (1)) are compared with two sets of experimental data: first, the large-scale, cold-flow, two-flap model data of reference 7; and second, the unpublished full-scale, hot-flow, three-flap model data obtained by using a TF-34 turbofan engine. Each configuration was positioned with the flaps in an approach attitude.

##### Cold-Flow, Two-Flap Model

The cold-flow model tests of reference 7 were conducted at the large-scale test facility schematically shown in figure 6. A primary airflow system supplied air to the 33-centimeter-diameter conical nozzle. The nozzle was located 7.33 nozzle diameters upstream of the flaps. Sound data were taken at nozzle exit Mach numbers of 0.5, 0.7 and 0.8 along the circumference of a 15.24-meter-radius microphone circle over a smooth blacktop ground plane.

The cold-flow model OASPL data are plotted as a function of radiation angle  $\theta$  measured from the nozzle inlet axis in figure 7. Discrete ground reflection effects were eliminated by matching acoustic data taken at ground level and at 3.58 meters above it. This procedure produced spectra which were essentially free-field plus 2.58 decibels. As shown in figure 7, the data were taken along an arc of the microphone circle from  $10^\circ$  to  $115^\circ$ . The data are restricted to this range of  $\theta$  because these are the limits of the useful impact noise data obtained in reference 13. A disproportionate increase in noise level with increased jet exit Mach number  $M_j$  is clearly shown between  $70^\circ \leq \theta \leq 115^\circ$ .

Overall-sound-pressure-level data taken at a jet Mach number  $M_j$  of 0.7 (from fig. 7) are compared in figure 8 with the total jet-flap impingement noise calculated from equation (1) (solid curve). Also included in figure 8 are estimates of each noise which contributes to the total impingement noise. These include trailing-edge noise applied to the second flap (eq. (2)), inflow noise applied to the two flaps and wing (eq. (3)), and the empirical estimate of the impact noise. The local gas properties and turbulence intensities used in the calculations were estimated, as in reference 7, from velocity decay profiles and small-scale turbulence intensities available in the literature.

From  $\theta = 10^\circ$  to  $80^\circ$  in figure 8, inflow noise from the second flap (having a  $U^6$  dependence) dominates the noise field; however, trailing-edge noise from the second flap (having a  $U^5$  dependence) is also a significant contributor. In the region from  $90^\circ$  to at least  $120^\circ$  impact noise (having a  $U^8$  dependence) is dominant, and inflow noise and trailing-edge noise do not significantly affect the noise level. The agreement between the measured data and the curve representing impingement noise (eq. (1)) in figure 8 is considered good.

In the lower portion of figure 8 the velocity exponents determined from the experimental data indicate that OASPL varies nominally as  $U^{5.6}$  for the range of  $\theta$  between  $10^\circ$  and  $70^\circ$ . Above  $80^\circ$ , however, OASPL varies as  $U^{6.6}$ ,  $U^{8.4}$ , and  $U^{7.3}$  at radiation angles of  $85^\circ$ ,  $100^\circ$ , and  $115^\circ$ , respectively. Comparing these results with the curves representing the dominant sound sources indicates general agreement with the expected values based on the present analysis.

Sound-pressure-level spectra. - A typical spectral plot for the cold-flow EBF configuration is presented in figure 9 (from ref. 7) for a radiation angle  $\theta$  of  $85^\circ$ . These data demonstrate the distinct broadband character of the sound field for values of jet exit Mach number  $M_j$  of 0.5, 0.7, and 0.8. Also shown in figure 9 are two tick marks positioned along each curve. These tick marks represent the frequencies at which two modal forms of the large-scale turbulence structures in a jet flow field are predicted to occur (ref. 15). Tick mark (1) represents the fundamental axisymmetric vortex mode (applicable at  $M_j < 0.35$ ), and tick mark (2) represents the first harmonic of the axisymmetric vortex mode. The parameters upon which these modes depend are given in reference 6.

The possibility that the large-scale turbulence structures in a jet flow field are associated (through transfer functions) with the dominant noise produced during jet impingement on a flat plate is considered in reference 6. It is shown in reference 6 that the first harmonic mode of these structures occurs at approximately the same frequency as the peak value of the far field sound pressure level. In figure 9, as with the flat plate data of reference 6, the data show that the first harmonic mode of these vortex structures (tick mark (2)) occurs at approximately the same frequency as the peak value of the spectra. Thus, the dominant noise produced by jet impingement on the

flaps appears to be associated with the large-scale turbulence structures in the jet flow field.

Plugs in slots. - In order to test the noise source model further, an effort was made to reduce substantially or eliminate the noise produced by inflow of the jet about the wing and flaps. Short spanwise covers, referred to as plugs, were placed over the slots between the wing and the first flap and between the first and second flaps with the flaps deployed (fig. 10). These plugs were smooth fairings positioned on the flaps and centrally located in relation to the intersection of the nozzle axis with the flaps. They had spanwise lengths of approximately 2 and 3 nozzle diameters (fig. 10) and were designed to prevent most of the impinging jet flow from passing through the spaces between the wing and the flaps. Thus, they redirected the jet flow over and downstream on the impingement side of the flaps and effectively reduced local inflow of the jet about the wing and flaps. The rest of the flap system in the spanwise direction was unaltered, which permitted normal aerodynamic operation of the flaps.

The OASPL distribution for the cold-flow model with plugs in the slots between the wing and flaps is presented in figure 11 (ref. 7). The calculated trailing-edge noise (eq. (2)) is also shown, along with the empirically based estimate of impact noise and the logarithmic sum of impact and trailing-edge noise  $OASPL_{\text{impact, TE}}$  (from eq. (5) of ref. 7), which is expressed by the following equation:

$$OASPL_{\text{impact, TE}} = 10 \log \left[ 10 \exp \left( \frac{OASPL_{\text{impact}}}{10} \right) + 10 \exp \left( \frac{OASPL_{\text{TE}}}{10} \right) \right] \quad (4)$$

Inflow noise is not included in equation (4) because of the assumption that the plugs effectively eliminate noise from this source.

At a jet Mach number of 0.7 (fig. 11) close agreement is shown between the measured data and the curve of  $OASPL_{\text{impact, TE}}$ . Trailing-edge noise (eq. (2),  $U^5$  dependence) is dominant between  $\theta = 10^\circ$  and  $40^\circ$ , while impact noise ( $U^8$  dependence) dominates from  $80^\circ$  to  $115^\circ$ . The dominance of these two noise sources is supported by the velocity exponents determined from the measured data and shown at the bottom of the figure.

#### Hot-Flow, Three-Flap Model

Figure 12 shows the full-scale, three-flap, swept-wing ( $25^\circ$  sweep angle) UTW EBF in an approach attitude (first, second, and third flaps in  $15^\circ$ ,  $35^\circ$ , and  $55^\circ$  position, respectively, ref. 8), using a TF-34 turbofan engine having a conical exhaust

nozzle with a 12-lobe, internal forced mixer. The axis of the nozzle intersected the leading edge of the third flap at approximately 4 nozzle diameters downstream from the exit plane of the nozzle. Also, the trailing-edge was oriented so that the included angle between a tangent to the flap surface and the jet axis was approximately  $55^\circ$ . The orientation of the engine to the three-flap swept-wing UTW EBF configuration was, therefore, not the same as that of the cold-flow model discussed in the preceding sections.

Overall-sound-pressure-level data taken at a jet Mach number of 0.5 are compared in figure 13 with the calculated estimate of the total jet-flap impingement noise (eq. (1)). The calculated impingement noise (solid curve) includes free-field estimates of trailing-edge noise applied to the third flap (eq. (2)), inflow noise applied to each of the three flaps (eq. (3)), and impact noise estimated from the data of reference 13. No velocity profile data were obtained at the trailing edge of the third flap in reference 8; thus the velocity profiles from the two-flap, cold-flow test data of references 6 and 7 were scaled up to estimate the boundary-layer height used in the calculations of trailing-edge noise. The local gas properties required in the calculations were determined from jet velocity profile and total temperature profile data for a conical exhaust nozzle with a 12-lobe internal forced mixer (unpublished data obtained from J. A. Schoenster of the Langley Research Center and N. E. Samanich of the Lewis Research Center). The local turbulence intensities in the vicinity of the flaps were estimated from the literature, as was done for the cold-flow model. The acoustic data were obtained by using 1.27-centimeter-diameter condenser microphones positioned on the ground.

In the region between  $\theta = 40^\circ$  and  $80^\circ$  in figure 13, inflow noise from the third flap (having a  $U^6$  dependence) dominates the noise field; however, trailing-edge noise from the third flap (having a  $U^5$  dependence) is also a significant contributor. In the region  $90^\circ$  to  $120^\circ$  impact noise (having a  $U^3$  dependence) is dominant, and inflow noise and trailing-edge noise do not significantly affect the total impingement noise level. For the three data points shown the calculated total impingement noise (eq. (1)) is within  $\pm 1.5$  decibels of the measured data.

In the lower portion of the figure the velocity exponents determined from the experimental data indicate that OASPL varied as  $U^{5.6}$  at radiation angles of  $70^\circ$  and  $90^\circ$ , but at  $110^\circ$  the dependence increased to  $U^{6.8}$ . Comparing these results with the curves representing the sound sources at  $70^\circ$ ,  $90^\circ$ , and  $110^\circ$  indicates that these nominal results and trend would be expected on the basis of the present analysis.

A spectral plot of the noise is presented in figure 14 for a radiation angle  $\theta$  of  $90^\circ$  and a jet exit Mach number  $M_j$  of 0.5. Also shown in figure 14 are the two tick marks representing the large-scale vortex modes discussed previously for the cold-flow model. The value of the jet exit velocity used in the calculations of the vortex mode frequencies is based on mass average flow conditions computed in the exit plane

of the nozzle. It is shown that the first harmonic mode of the large-scale turbulence structures in the jet flow field (tick mark ②) occurs at approximately the same frequency as the peak value of the sound spectra. Thus, as with the cold-flow model, the dominant noise produced by jet impingement on the flaps appears to be associated with the large-scale turbulence structures in the jet flow field.

#### CONCLUDING REMARKS

An analytical expression has been developed which approximates the overall sound pressure level and directivity of data obtained from two large-scale UTW EBF configurations in an approach attitude. Three dominant noise sources are modeled; two are based on analytical theories, and the third is based on scaled experimental data. The noise sources include the following: first, impact noise produced by the jet exhaust impinging on the surface of the most downstream flap; second, inflow noise, produced by the jet exhaust flow about the wing and flaps, which in turn produces a fluctuating lift response to an upwash disturbance; and third, trailing-edge noise, produced by the jet flow passing over the trailing edge of the most downstream flap.

The analysis was compared with experimental data obtained by using a subsonic cold-air jet impinging on a two-flap wing and a subsonic hot-gas jet from a TF-34 turbofan engine impinging on a three-flap swept wing. The agreement between the analytical expression and the data is considered good in both cases.

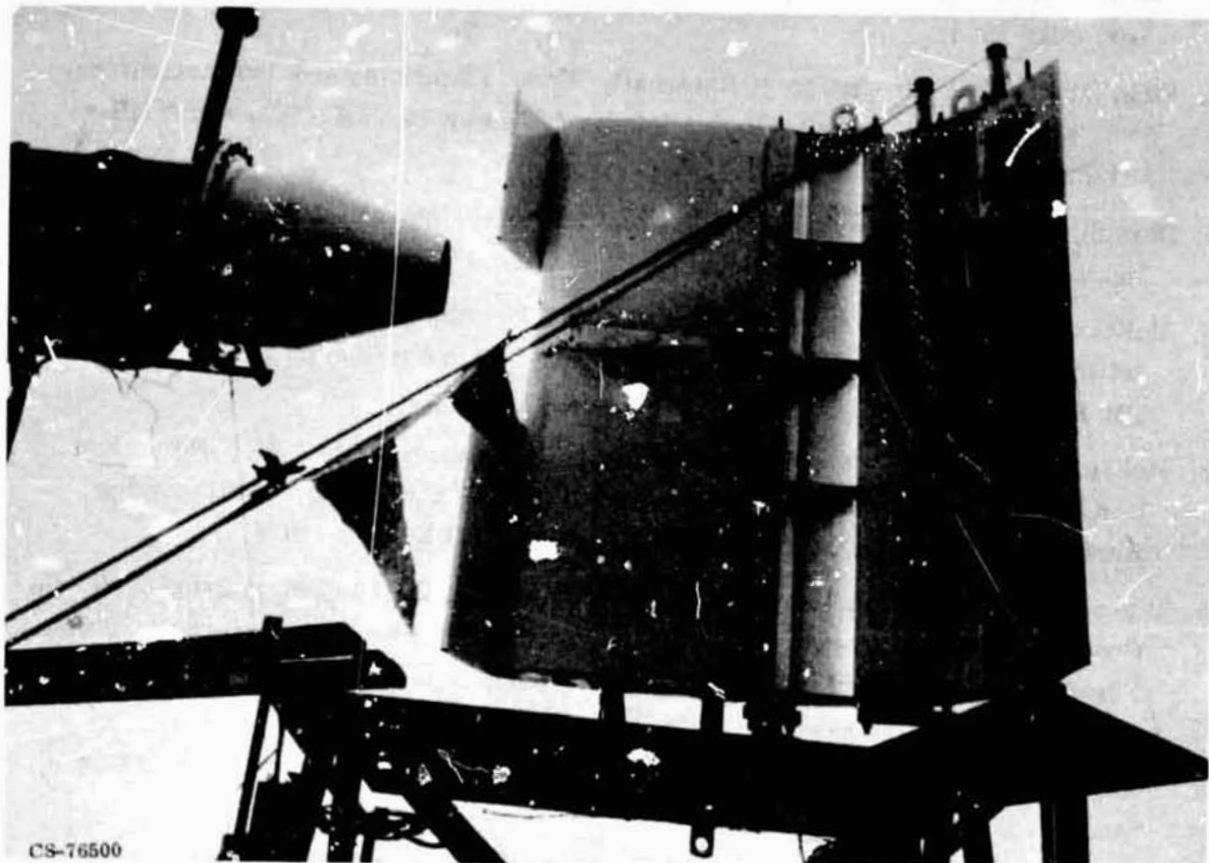
The dominant noise at  $90^\circ$  under the wing appears to result from the jet impact (eighth power dependence on jet velocity) rather than a fluctuating lift dipole (sixth power) or a trailing-edge disturbance (fifth power).

The frequency at which the peak sound pressure level occurred appears to be governed by the periodic formation and shedding of large-scale turbulence structures (ring vortices) from the outlet of the jet nozzle.

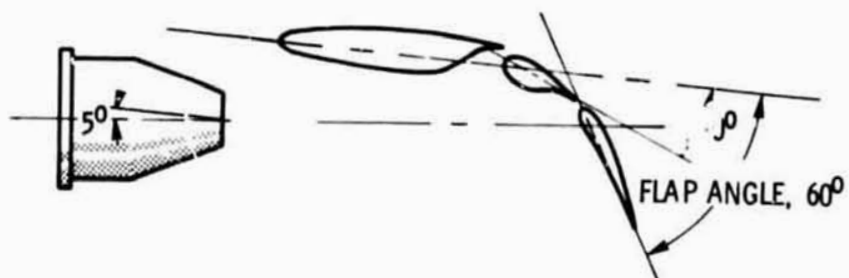
#### REFERENCES

1. Maglieri, Domenic J.; and Hubbard, Harvey H.: Preliminary Measurements of the Noise Characteristics of Some Jet-Augmented-Flap Configurations. NASA Memo 12-4-58L, 1959.
2. Dorsch, R. G.; Krejsa, E. A.; and Olsen, W. A.: Blown Flap Noise Research. AIAA Paper 71-745, June 1971.

3. Dorsch, R. G.: Externally Blown Flap Noise Research. SAE Paper 740468, Apr. - May 1974.
4. Fink, Martin R. Prediction of Externally Blown Flap Noise and Turbomachinery Strut Noise. (United Technologies Research Center, NAS3-17863) NASA CR-134883, 1975.
5. Dorsch, Robert G.; Clark, Bruce J.; and Reshotko, Meyer: Interim Prediction Method for Externally Blown Flap Noise. NASA TM X-71768, 1975.
6. McKinzie, Daniel J., Jr.; and Burns, Robert J.: Analysis of Noise Produced by Jet Impingement Near the Trailing Edge of a Flat and a Curved Plate. NASA TM X-3171, 1975.
7. McKinzie, Daniel J., Jr.; Burns, Robert J.; and Wagner, Jack M.: Noise Reduction Tests of Large-Scale-Mode Externally Blown Flap Using Trailing-Edge Blowing and Partial Flap Slot Covering. NASA TM X-3379, 1975.
8. Samanich, N. E.; Heidelberg, L. J.; and Jones, W. L.: Effect of Exhaust Nozzle Configuration on Aerodynamic and Acoustic Performance of an Externally Blown Flap System with a Quiet 6:1 Bypass Ratio Engine. AIAA Paper 73-1217, Nov. 1973.
9. Fink, M. R.: Mechanisms of Externally Blown Flap Noise. AIAA Paper 73-1029, Oct. 1973.
10. Guinn, Willy A.; Blankey, Dennis F.; and Gibson, John S.: V/STOL Noise Prediction and Reduction. LG73ER0062, Lockheed-Georgia Co. (FA 3D-73-145), 1973.
11. Ffowcs, William, J. E.; and Hall, L. H.: Aerodynamic Sound Generation by Turbulent Flow in the Vicinity of a Scattering Half Plane. J. Fluid Mech., vol. 40, pt. 4, Mar. 1970, pp. 657-670.
12. Hayden, Richard E.: Noise from Interaction of Flow with Rigid Surfaces: A Review of Current Status of Prediction Techniques. NASA CR-2126, 1972.
13. Olsen, William A.; Miles, Jeffrey H.; and Dorsch, Robert G.: Noise Generated by Impingement of a Jet Upon a Large Flat Board. NASA TN D-7075, 1972.
14. Dorsch, R. G.; Kreim, W. J.; and Olsen, W. A.: Externally Blown-Flap Noise. AIAA Paper 72-129, Jan. 1972.
15. Neuwerth, Gunther: Acoustic Feedback Phenomena of the Subsonic and Hypersonic Free Jet Impinging on a Foreign Body. NASA TT F-15719, 1974.



(a) Test installation.



(b) Approach attitude.

Figure 1.- Cold-flow model of two-flap EBF with conical nozzle.

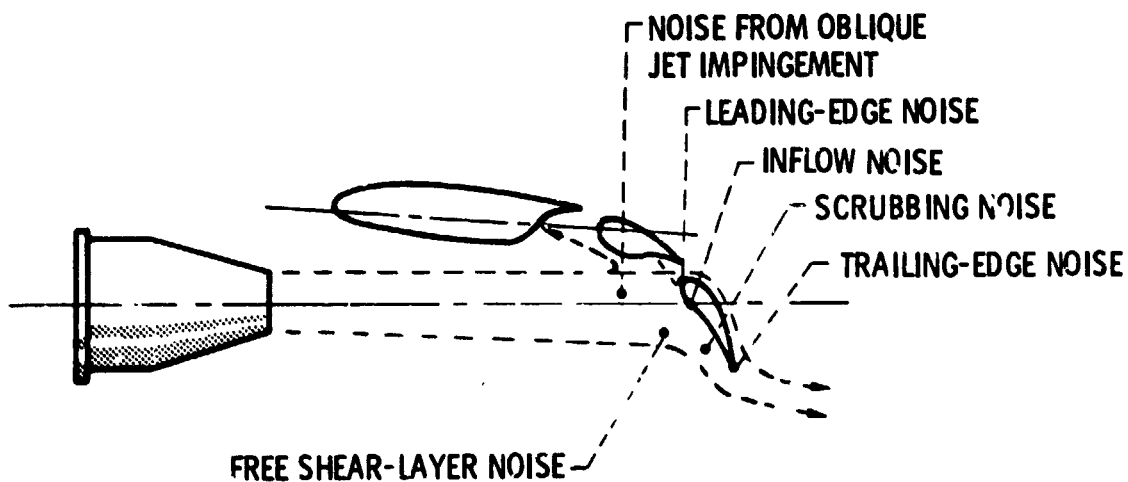


Figure 2.- Noise sources resulting from jet impingement on EBF two-flap wing in its approach attitude.

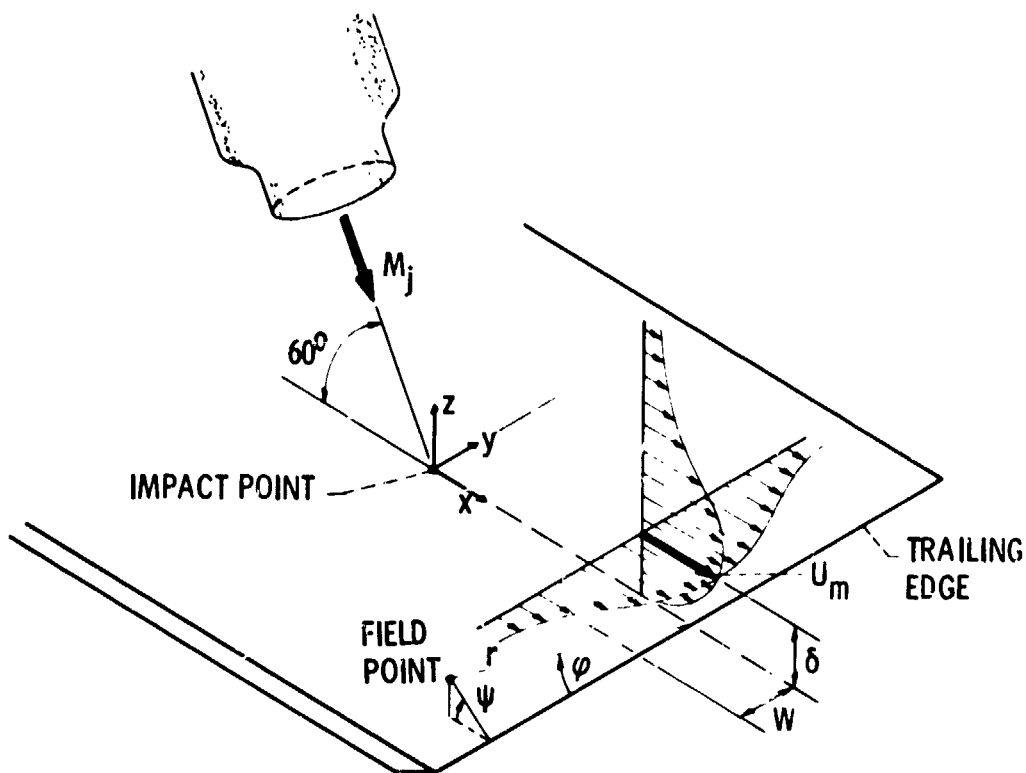


Figure 3.- Coordinate system of jet impinging on semi-infinite half-plane near its trailing edge (ref. 6).

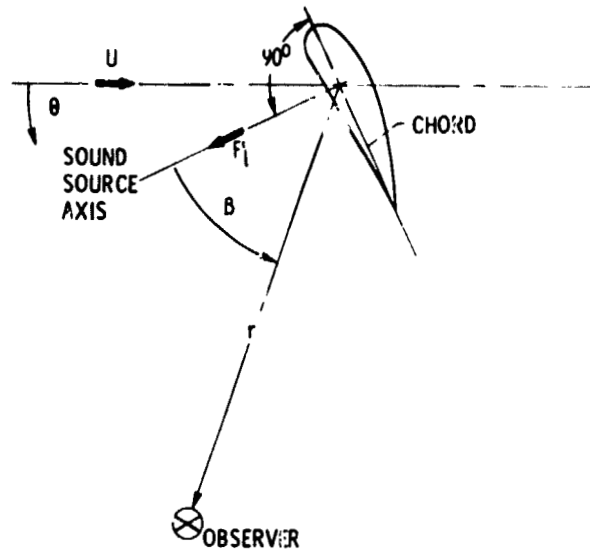


Figure 4.- Coordinate system for inflow noise (ref. 7).

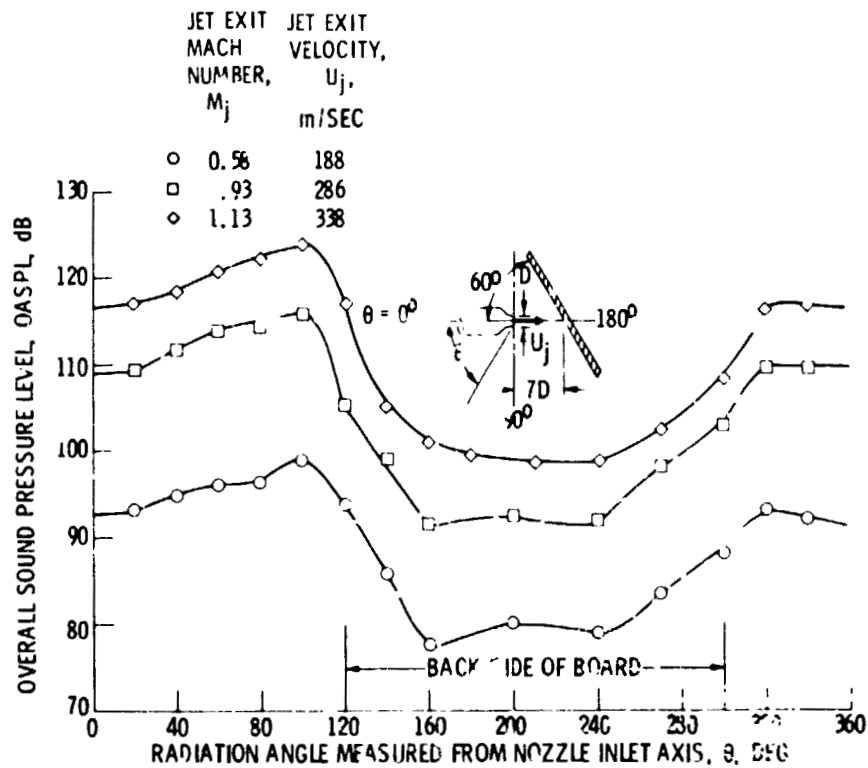


Figure 5.- Overall-sound-pressure-level distribution for large flat board.  $D = 5.2$  m; microphone radius,  $0.05$  m; azimuthal angle,  $0^\circ$  (ref. 13).

REPRODUCIBILITY OF THE ORIGINAL PAGE IS POOR

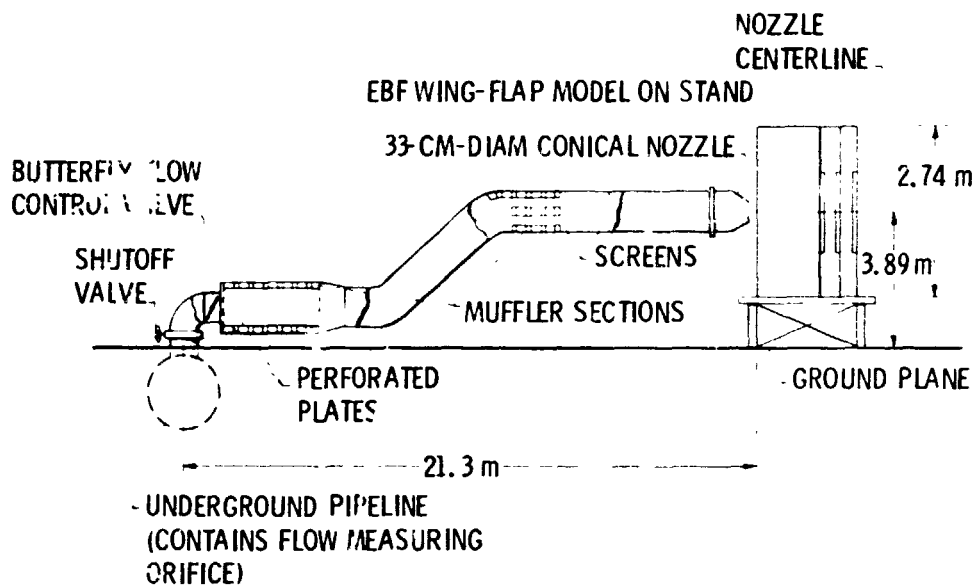


Figure 6.- Diagram of EBF large-scale test facility showing primary airflow system (ref. 7).

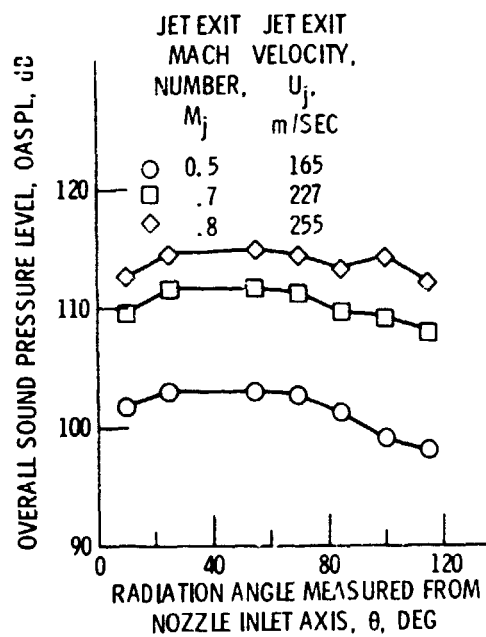


Figure 7.- Overall-sound-pressure-level distribution for two-flap EBF cold-flow configuration with 30° to 60° flaps (approach attitude). Microphone radius, 15.24 m.

C-4

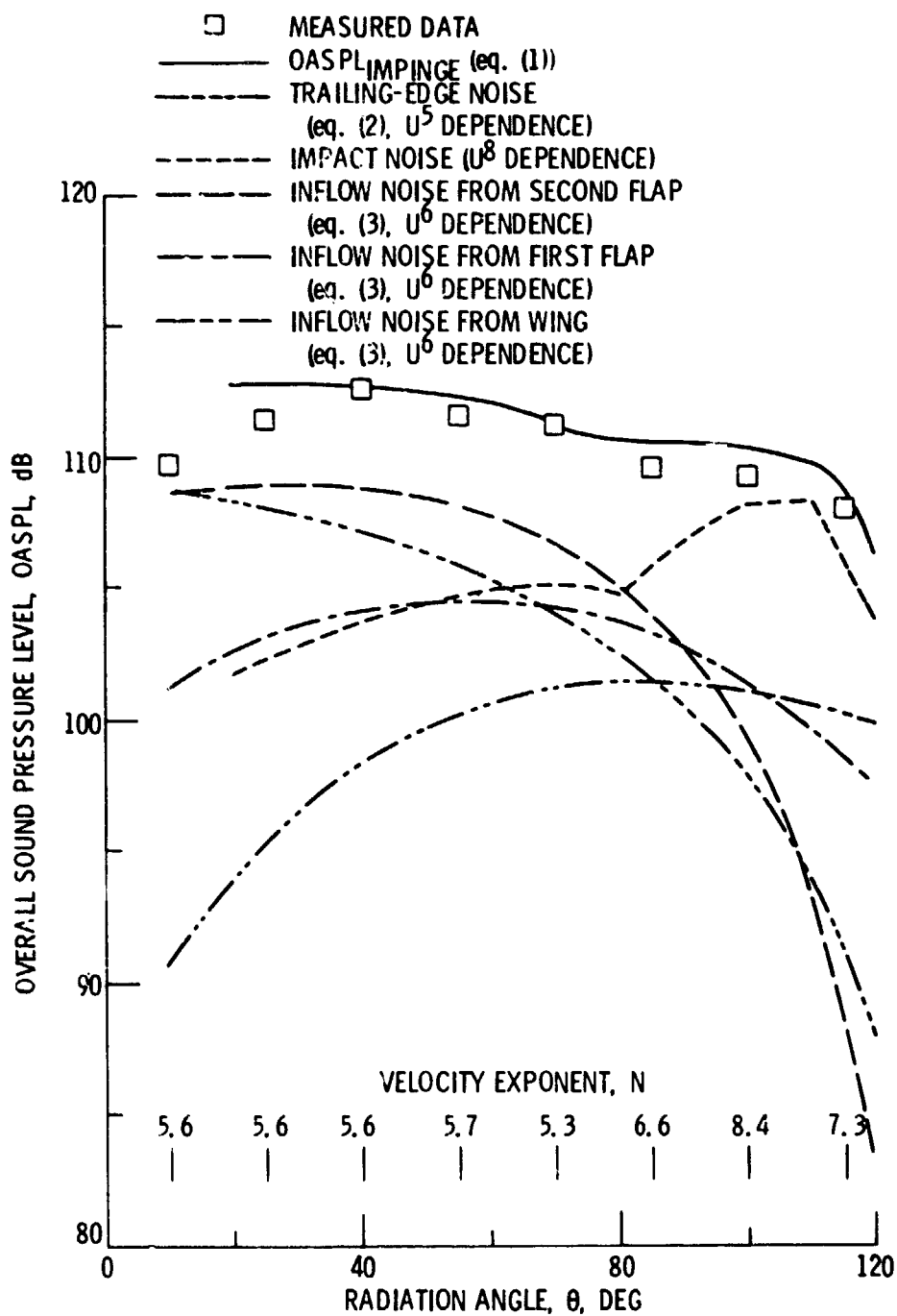


Figure 8.- Comparison of measured and calculated overall sound pressure level for cold-flow configuration (approach attitude).  $M_j = 0.7$ ;  $U_j = 227$  m/sec (ref. 7); microphone radius, 15.24 m.

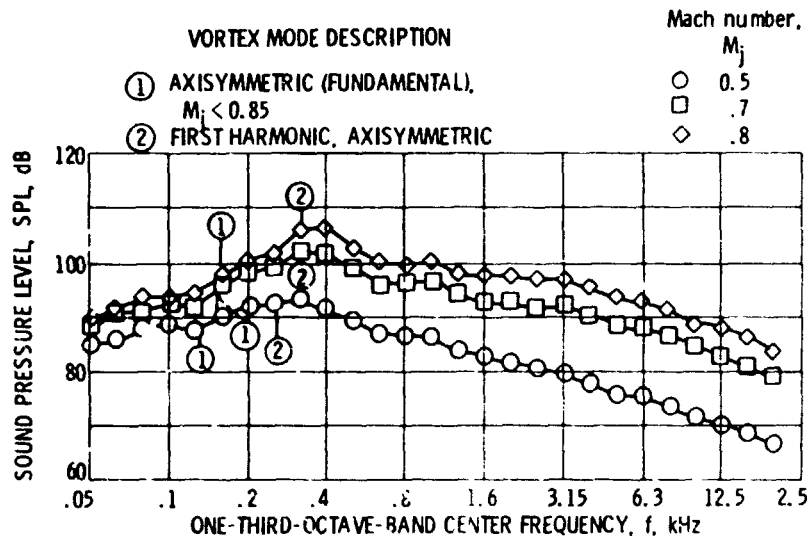


Figure 9.- Sound-pressure-level spectra for two-flap EBF cold-flow configuration with  $30^\circ$  to  $60^\circ$  flaps (approach attitude).  $\theta = 85^\circ$  (ref. 7); microphone radius, 15.24 m.

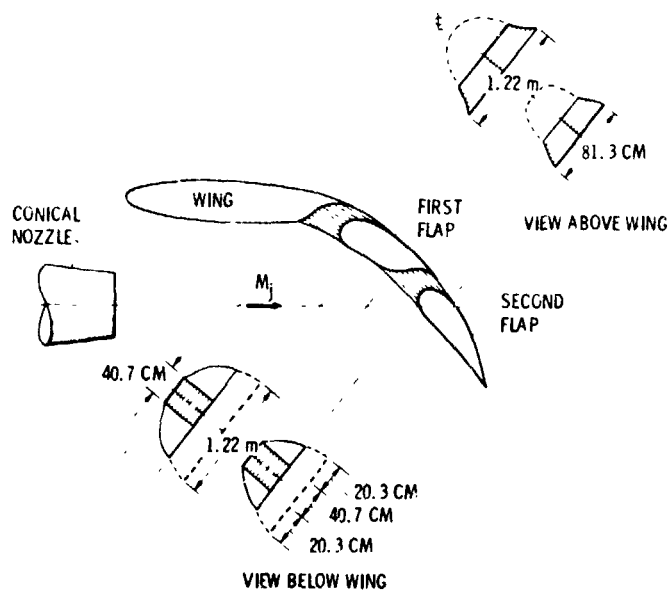


Figure 10.- Plug fairings in slots between wing and first flap and first and second flaps (ref. 7).

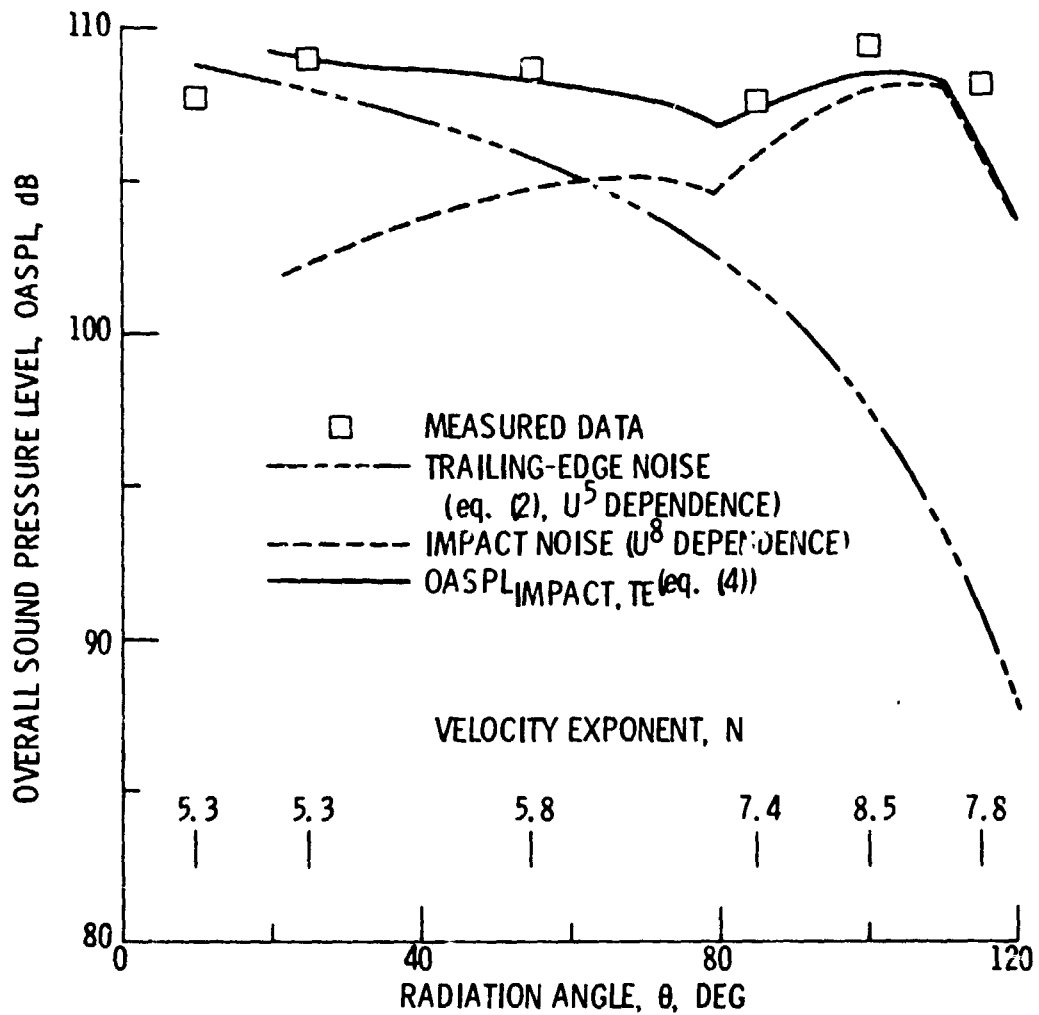
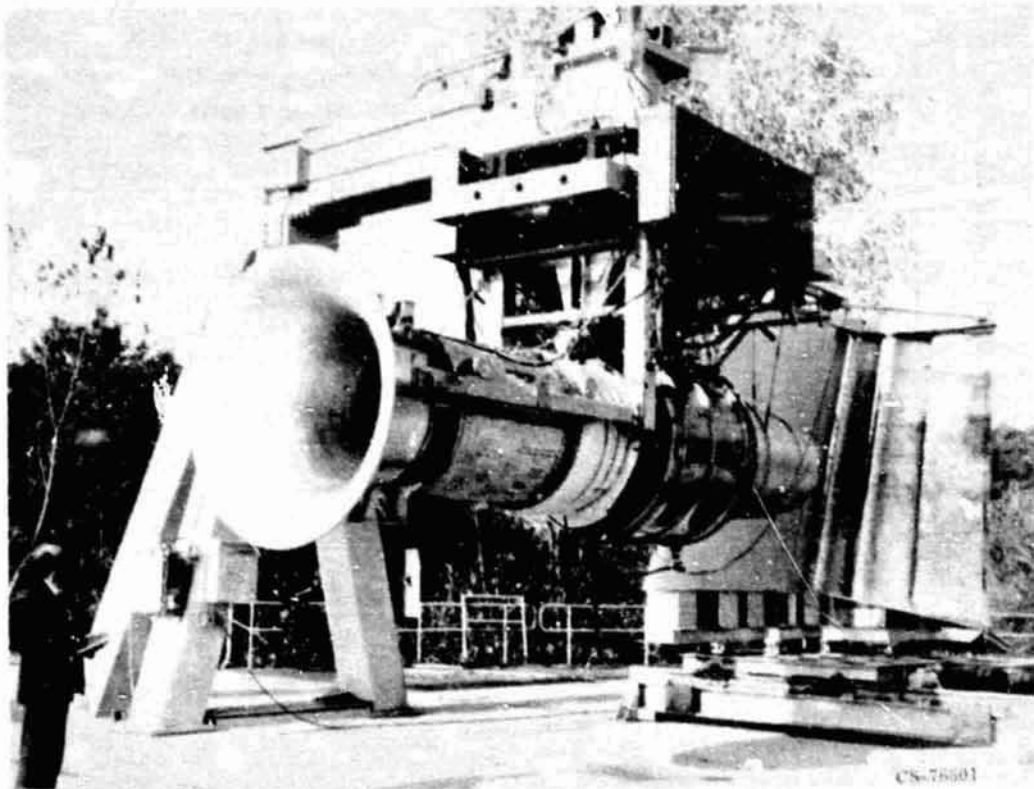
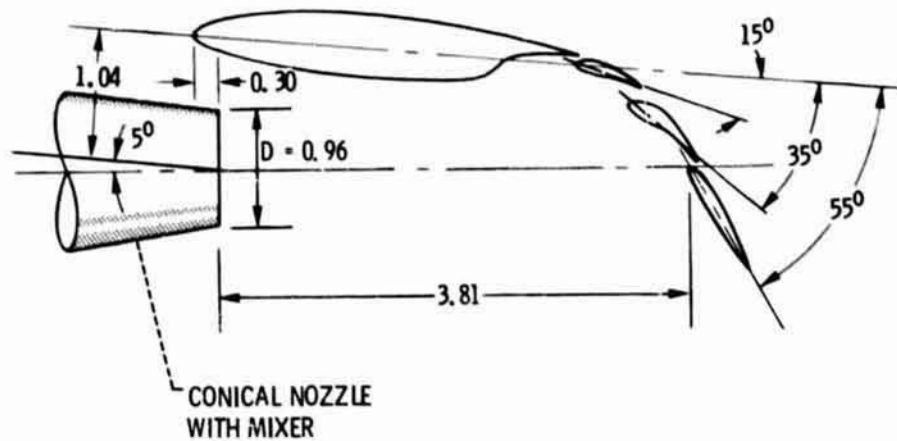


Figure 11.- Comparison of measured and calculated overall sound pressure level for cold-flow configuration with plugs (approach attitude).  $M_j = 0.7$ ;  $U_j = 227$  m/sec (ref. 7); microphone radius, 15.24 m.



(a) Test installation.



(b) Approach attitude.

Figure 12.- Hot-flow model of three-flap EBF with TF-34 turbofan engine (ref. 8). (All dimensions in meters.)

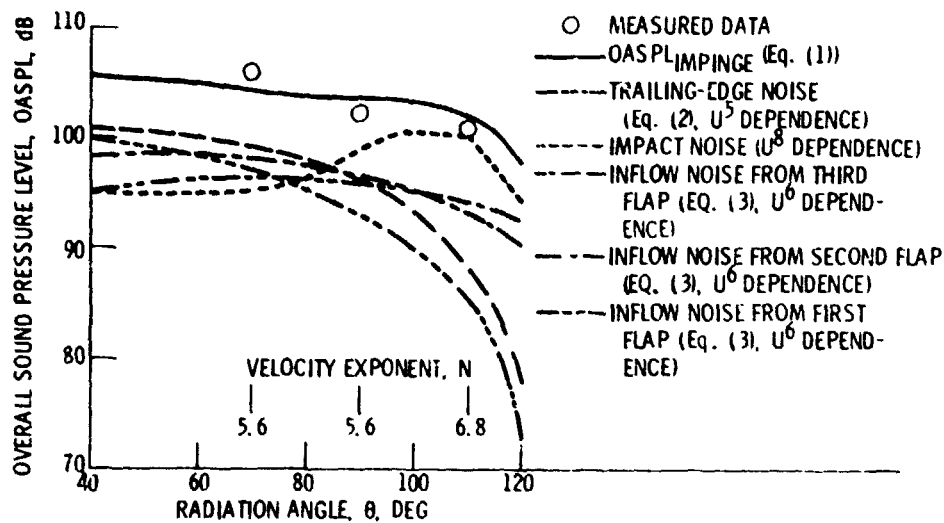


Figure 13.- Comparison of measured and calculated free-field overall sound pressure level for full-scale three-flap configuration with TF-34 turbofan engine (approach attitude).  $M_j = 0.5$ ; jet exit core velocity, 250 m/sec; core temperature, 749 K; microphone radius, 30.48 m.

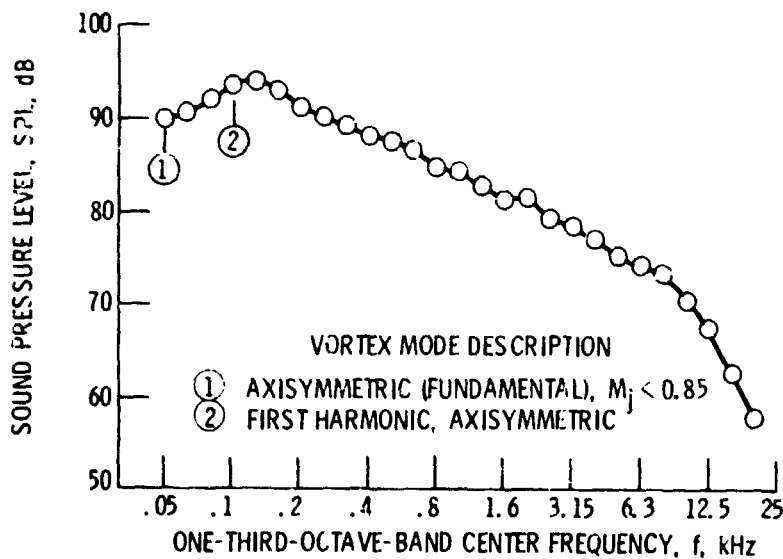


Figure 14.- Measured free-field sound pressure level spectra for full-scale three-flap configuration with TF-34 turbofan engine (approach attitude).  $M_j = 0.5$ ;  $\theta = 90^\circ$  (ref. 8); microphone radius, 30.48 m.